UNSYS digital

International Journal of Robotics and Mechatronics

Design, Kinematic, Dynamic, and Stiffness Analysis of A 5-DOF Single-Incision Laparoscopic Surgery Robot

Heqiang Tian†, Chenling Zheng†, Jiakun Jiang†, Jianyong Li†, Yan Li‡, Yanan Yao†

†College of Mechanical and Electronic Engineering, Shandong University of Science and Technology, China.

‡Network security and Information Office, Shandong University of Science and Technology, China.

Abstract— In order to further reduce the incisions of laparoscopic surgery and the possibility of infection, the organic combination of single-incision laparoscopic surgery (SILS) and robotics has made the degree of minimally invasive surgery further improved. A new 5-DOF single-incision laparoscopic surgery robot was designed based on Axiomatic Design Theory, whose structure consisting of the movement mechanism, the endoscope and the position and pose adjustment mechanism. The robot parts are connected in series and parallel, allowing a pivotal motion of the endoscope in the center of the robot for realizing the incision. In order to achieve a performance optimization and a dynamic control of the single-incision laparoscopic surgical robot, the kinematics and dynamic modeling and dynamic stiffness analysis of the robot are especially important. The forward kinematics equation, inverse kinematics equation and Jacobian matrix of the SILS robot are derived based on D-H method and geometric method, and the kinematics numerical simulation is carried out by Matlab. The dynamic equation of the robot is derived by Kane method. Subsequently, a numerical simulation of the robot dynamics equation is performed, with its virtual prototype utilized to set the motion plan of the robot mechanism. After robot's dynamic simulation, the numerical changes of the driving force and torque for each robot's moving mechanism are obtained. The performed simulation results further verify the correctness of the established robot's dynamic model. Finally, utilizing the above methods, the dynamic stiffness model and evaluation index of the robot are determined, and the dynamic stiffness of the robot is analyzed and evaluated. The results of the kinematics, dynamic and stiffness analysis of the SILS robot further validate that the 5-DOF SILS robot has a reasonable structure, motion and sufficient stability to meet the needs of single-incision laparoscopic surgery.

Keywords— abdominal surgical robot, axiomatic design theory,kinematics,dynamics,stiffness

DOI: 10.21535/ijrm.v7i1.1031

I. INTRODUCTION

THE single-incision laparoscopy is a minimally invasive surgical procedure that is currently used by surgeons and is considered a new innovation modality in the field of laparoscopic surgery. However, due to the field of view occlusions of single-incision laparoscopic surgery several challenges are introduced during the operation.Some of them include the interference problem of surgical instruments that cause poor operational freedom of surgery, the difficulty in estimating the distance and depth of the lesions, the poor visibility of the surgical field, as well as the even higher necessary surgeon's laparoscopic operation experience. The critical combination of laparoscopic surgery and robotic technology effectively solves the problems of conventional laparoscopic surgeries, and the degree of invasive surgery is further reduced. Recently, the research in abdominal surgical robots has been expandingresulting in various structural forms of robots, such as AESOP surgical robots[1], ZEUS surgical robots[2], EndoAssist surgical robots[3], Da Vinci surgical robots [4], single-channel Snake-Like Robot[5] and single-incision dual-arm small robot IREP[6].

However, the minimally invasive single-incision laparoscopic surgical robots entail a complicated structure, poor stability, difficult control, and provide a very confined space to the surgeon for performing the surgical operation.Therefore, a new SILS robot need to be proposed, which can control the endoscope to enter the human body cavity through a narrow single hole with relatively rigid and stable relative to human tissues and organs. Besides the reasonable structure and adequate motion degree of freedom, the designed robot should have the ability to work normally in a certain continuous space and the ability to change its attitude within a given range, so as to avoid important tissues during the operation. It should also have better flexibility and stiffness, and have the best motion and force transfer performance in the motion trajectory.

In this paper, a new 5-DOF SILS robot is designed based on Axiomatic Design Theory firstly. And, the forward kinematics equation, inverse kinematics equation and Jacobian matrix of the SILS robot are derived based on D-H method and geometric relationship, and the kinematics numerical simulation is carried out by Matlab. In order to address the performance optimization and dynamic control of the single-incision laparoscopic surgical robot, the dynamic modeling and dynamic stiffness analysis of the robot are required[7]-[10]. The dynamic equations of robots are quite difficult to obtain with the most commonly used modeling methods including the virtual work principle, Newton Euler method and Lagrangian method, Kane method[11]-[19]. The Kane method[20] requires to project the vector force and the

Corresponding author: Heqiang Tian (e-mail: thq_1980@126.com)
579 Qianwangang Road, Huangdao District, Qingdao,
Shandong Province, 266590, China.

This paper was submitted on August 27, 2019, and accepted on August 28, 2019.

D'Alembert inertial force into a special base vector, so that the ideal binding force is not generated in the equation, thereby improving the computational efficiency of the equation. In this paper, the inverse kinematics equation and the Jacobian matrix of the robot are derived by a geometric method with its dynamic model being extracted by the Kane method. Based on the motion sequence of each mechanism of the robot, the motion planning of different time series is then proposed. The numerical and virtual simulations are carried out by MATLAB and ADAMS, respectively, to further verify the correctness of the dynamic model. Finally, the dynamic stiffness model and the evaluation index of the robot are defined, allowing an analysis and evaluation of robot's dynamic stiffness.

By replacing the doctor with a surgical robot's end-effector to hold the surgical instrument, the quality and accuracy of the operation are improved, and the surgical operation is expanded [25, 26]. SILS robot needs to meet the requirements of operation in terms of composition, dexterity, freedom and stability. The robot should include two independent parts: robot positioning mechanism and endoscope pose adjusting mechanism; the endoscope pose adjusting mechanism should have high flexibility to locate the surgical incision and reduce the interference of other mechanisms; the endoscope needs to achieve 3 DOF motion, so as to fully obtain the target vision in the abdominal cavity; the various mechanisms of the robot should be positioned at the surgical incision with smooth motion and enough stiffness.

II. Laparoscopic Surgical Robot Design

This section presents a design requirement, design method and mechanical structure of a single-incision laparoscopic surgical robot.

A. Robot design requirement

Traditional laparoscopic surgery usually uses a 2-4 incisions method. Surgeons use forceps to enter the abdominal cavity through a trocar (about 5-10 mm in diameter) and observe the images obtained by endoscope thatneed to be adjusted to meet the doctor's vision requirements (**Figure 1(a)**), which results in multiple long scars on the patient's abdomen[21][22]. Because of the limitation of endoscopy in traditional laparoscopic surgery, considering the safety of the operation process and avoiding the patient's body injury caused by endoscope motion, the endoscopy should achieve three-degree-of-freedom motion centered on the surgical incision[23][24]: two degrees of freedom of cone swinging centered on the operation incision and moving along the axis of the endoscope, as shown in **Figure 1(b).**

B. Design based on axiomatic design theory

Axiomatic design theory is a scientific criterion in the field of design to make correct decisions in the design process by guiding designers, which provides a good way of thinking for innovative design or improvement of existing design[27]. Axiomatic design divides the design process into four domains, namely, Customer domain, Functional domain, Physical domain and Process domain. In axiomatic design, a direct mapping relationship between functional domain and physical domain is established, where a function is directly corresponding to a structure, as shown in Figure 2.

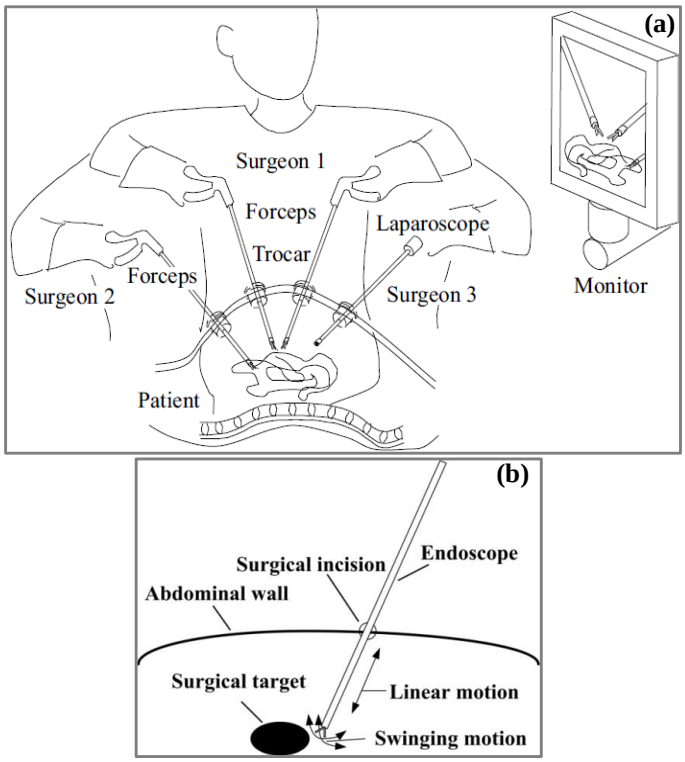

Figure 1 (a) Conventional laparoscopic surgery, and (b) Motion mode of endoscope

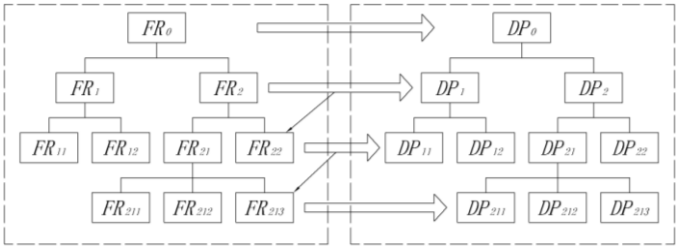

Figure 2 Mapping principle of functional domain to physical domain

Customer requirements are defined as functional requirements (FR), and design solutions are defined as design parameters (DP) that should satisfy FR. The design process can be seen as a mapping from functional requirement domain to design parameter domain. Mapping can be expressed by axiomatic design theory as follows:

$$\{\mathrm{FRs}\} = [\mathrm{A}]\{\mathrm{DPs}\} \quad (1)$$

Formula (1) is called product design equation, in which {FRs} is the function requirement vector, {DPs} is the design parameter quantity, [A] is the product design matrix based on FR and DP, and the design process of the robot is guided by [A]. Formula (1) is called product design equation, in which {FRs} is the function requirement vector, {DPs} is the design parameter quantity, [A] is the product design matrix based on FR and DP, and the product design process is guided by [A]. According to the different forms of [A], design can be divided into three types:

(1) Uncoupled Design: [A] is a diagonal matrix;

(2) Decoupled Design: [A] upper triangular or lower triangular matrix;

(3) Coupled Design: [A] is neither triangular nor diagonal matrix.

Axiomatic design is a structural design method. Its purpose is to improve design behavior by establishing criteria for evaluating potential design activities and providing means to implement these criteria. These criteria are: independence axiom and information minimization axiom. Independence axiom refers to maintaining the independence of FRs and pointing out the relationship between FRs and DPs. The design scheme must satisfy each independent functional requirement without affecting other functional requirements, that is, the relationship between FR and DP should be uncoupled or decoupled. Information axiom means that under the condition of satisfying the axiom of independence, the design with the smallest amount of information is the optimal design. For the same design task, different designers may come up with different design schemes. It is also possible that these schemes satisfy the independent axiom. The design with the least information content should be the best design in evaluation.

Axiomatic design can effectively guide designers to complete innovative design. In this paper, a new type of SILS robot is designed by using axiomatic design theory. SILS robot's endoscope can locate the patient incision and complete two degrees of freedom of cone swinging with the center of the operative incision and moving along the axis of the endoscope. Therefore, in order to design a new SILS robot, especially the robot structure, the functional requirements are as follows:

- FR1: Realize the functional strategy of SILS robot;
- FR2: Drive the mechanism of SILS robot;
- FR3: Control the motion of SILS robot;
- FR4: Real-time monitoring of the motion of SILS robot.

According to the above functional requirements of the robot, the corresponding design parameters are as follows:

- DP1: Mechanical system;
- DP2: Driving system;
- DP3: Control system;
- DP4: Monitoring system.

According to axiomatic design principle, design matrix can be obtained, and the relationship between FR and DP can be expressed as follows:

$$\begin{bmatrix} \mathrm{FR1} \\ \mathrm{FR2} \\ \mathrm{FR3} \\ \mathrm{FR4} \end{bmatrix} = \begin{bmatrix} X & X & & \\ & X & & \\ & & X & \\ & & & X \end{bmatrix} \begin{bmatrix} \mathrm{DP1} \\ \mathrm{DP2} \\ \mathrm{DP3} \\ \mathrm{DP4} \end{bmatrix} \quad \textbf{(2)}$$

FR2, FR3 and FR4 can be satisfied independently, while FR1 needs to be satisfied by DP1 and DP2. It can be seen from (2) that the design matrix is decoupled, so it conforms to the independent axiom of axiomatic design principle.

In order to realize the various motions of SILS robot, FR1 can be decomposed into the following two requirements:

- FR11: Realize the localization of robot endoscope;
- FR12: Realize the pose adjustment of robot endoscope.

To meet the requirements of FR1, the design parameter DP1 can be decomposed into:

- DP11: A robot endoscope positioning mechanism;
- DP12: Arobot endoscope pose adjustment mechanism.

According to axiomatic design principle, design matrix can be obtained, and the relationship between FR and DP can be expressed as follows:

$$\begin{bmatrix} \mathrm{FR11} \\ \mathrm{FR12} \end{bmatrix} = \begin{bmatrix} X & \\ & X \end{bmatrix} \begin{bmatrix} \mathrm{DP11} \\ \mathrm{DP12} \end{bmatrix} \quad \textbf{(3)}$$

Equation (3) shows that the design matrix is uncoupled and accords with the independent axiom of axiomatic design principle.

To realize the localization of robot endoscope, FR11 can be decomposed into three sub-functions as follows:

- FR111: Endoscope positioning mechanism realizes horizontal motion of endoscope (X direction);
- FR112: Endoscope positioning mechanism realizes the vertical motion of endoscope (Y direction);
- FR113: Endoscope positioning mechanism realizes the anterior and posterior motion of endoscope (Z direction).

In order to meet the requirements of FR11, DP11 is decomposed into the following parts according to axiomatic design theory:

- DP111: A double-track single screw sliding table mechanism with horizontal arrangement;
- DP112: A double guide rail double screw sliding table mechanism with vertical arrangement;
- DP113: A parallel mechanism consisting of two sliders mounted on the vertical slide screw and two connecting rods articulated.

According to axiomatic design principle, design matrix can be obtained, and the relationship between FR and DP can be expressed as follows:

$$\begin{bmatrix} \mathrm{FR111} \\ \mathrm{FR112} \\ \mathrm{FR113} \end{bmatrix} = \begin{bmatrix} X & & \\ & X & \\ & & X \end{bmatrix} \begin{bmatrix} \mathrm{DP111} \\ \mathrm{DP112} \\ \mathrm{DP113} \end{bmatrix} \quad \textbf{(4)}$$

In order to adjust the attitude of robot endoscope, FR12 can be decomposed into the following two sub-functions:

- FR121: Pose adjusting mechanism realizes swing forward and backward of endoscope (Z direction);

- FR122: The pose adjustment mechanism realizes swing left and right of endoscope (X direction).

In order to meet the requirements of FR12, DP12 is decomposed into the following parts according to axiomatic design theory:

- DP121: A mechanism in which long fork and cross base can rotate relatively;
- DP122: An endoscope rotating mechanism driven directly by a motor.

According to axiomatic design principle, design matrix can be obtained, and the relationship between FR and DP can be expressed as follows:

$$\begin{bmatrix} \text{FR121} \\ \text{FR122} \end{bmatrix} = \begin{bmatrix} X & \\ & X \end{bmatrix} \begin{bmatrix} \text{DP121} \\ \text{DP122} \end{bmatrix} \quad \textbf{(5)}$$

From (4) and (5), it can be seen that the design matrix is uncoupled and accords with the independent axiom of axiomatic design principle.

C. *Mechanical structure description*

According to the axiomatic design above, a new rectangular coordinate structure is selected as the main configuration of the robot, whose degree of freedom is 5, including 3 degrees of freedom of motion and 2 degrees of freedom of rotation. The new robot mechanism sketch is shown in Figure 3. The robot structure is divided into a robot positioning mechanism with 3 degrees of freedom and an endoscope pose adjustment mechanism with 2 degrees of freedom. The robot positioning mechanism can realize the positioning of the endoscope to the incision of the patient's abdominal cavity, and the endoscope moves to the corresponding incision position through the horizontal and vertical motions. The positioning mechanism of the robot which includes a horizontal motion mechanism and a vertical motion mechanism adopts a screw transmission mechanism. The horizontal moving mechanism is a horizontally arranged double guide single spiral screw slide table. The effective stroke of the sliding table is 300 mm. The vertical moving mechanism is a double guide double spiral screw slide table arranged in a vertical direction, which is integrally mounted on a slide table of a horizontal moving mechanism and a parallel mechanism that two sliders in the vertical motion mechanism are connected by links to form realizes the axis motion. The effective length of the vertical moving mechanism is 400 mm. The robot pose adjustment mechanism is driven by two mutually perpendicular motors. A motor is mounted on the first long fork, the motor output shaft is connected to a cross-rotation base, the rotation angle range is 0° ~ 120°, and the other motor is mounted on the cross-rotation base, and the rotation angle range is 0° ~ 60°. The structure model of the laparoscopic surgery robot was obtained, as shown in Figure 3(b).

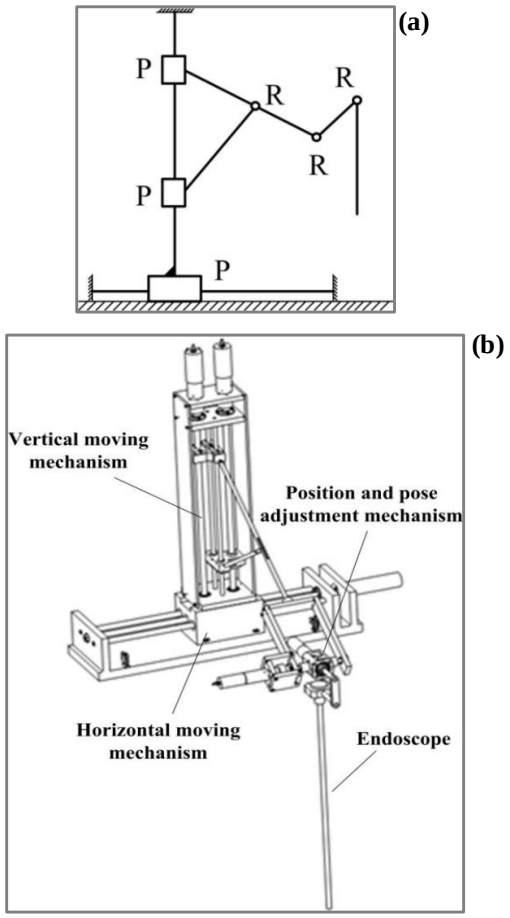

Figure 3 (a) Schematic diagram of mechanism and (b) 3D schematic representation of SILS robot

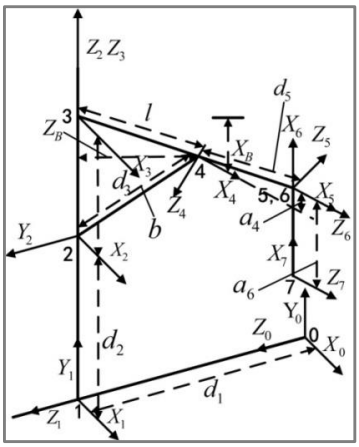

Figure 4 Coordinate system of the SILS robot mechanism

III. Kinematic of Laparoscopic Surgical Robot

A. *Forward kinematics*

The SILS robot in Figure 3 is an open kinematic chain. The D-H method [28] can be used to establish forward kinematics equation by the equivalent homogeneous transformation matrix from coordinate system of the base to coordinate system of the end-effector. The SILS robot adopts a series-parallel hybrid structure with 5 degrees of freedom, which can realize endoscope positioning, axis telescopic motion along and axis conical motion. The parallel part of the robot mechanism can be simplified for the same joint to form a series part, and the coordinate transformation of each joint can be obtained, as shown in Figure 4. The parallel part is fused into the series part by geometric relation, and then the forward kinematics solution

of the SILS robot can be obtained. For the parameters of the rods, α_{i-1} is defined for the rotation angle between the two joint axes, a_{i-1} is the vertical length of the rod between the two joint axes, d_i is the vertical offset of the rod between the two joint axes, and θ_i is the perpendicular joint angle between the two joint axes. The rod parameters and joint variables of the robot are shown in Table 1.

Table 1 Robot link parameters and joint variables

No.	α_{i-1}	a_{i-1}	d_i	θ_i
1	0°	0	d_1	0°
2	-90°	0	d_2	0°
3	0°	0	d_3	0°
4	90°	Z_B	X_B	θ_4
5	-180°	a_4	d_5	θ_5
6	90°	0	0	90°
7	0°	a_6	0	0°

According to the parameters and joint variables between adjacent joint coordinate systems, the transformation matrices of each rod are obtained. By multiplying the transformation matrices of the rods, the robot end transformation matrices in coordinate system of the base {O} can be obtained as follows:

$$
{}^{0}_{1}T=\begin{bmatrix}1&0&0&0\\0&1&0&0\\0&0&1&d_1\\0&0&0&1\end{bmatrix};\quad
{}^{1}_{2}T=\begin{bmatrix}1&0&0&0\\0&0&1&d_2\\0&-1&0&0_1\\0&0&0&1\end{bmatrix};
$$

$$
{}^{2}_{3}T=\begin{bmatrix}1&0&0&0\\0&1&0&0\\0&0&1&d_3\\0&0&0&1\end{bmatrix};\quad
{}^{3}_{4}T=\begin{bmatrix}1&0&0&Z_B\\0&0&-1&-X_B\\0&1&0&0\\0&0&0&1\end{bmatrix};
$$

$$
{}^{4}_{5}T=\begin{bmatrix}1&0&0&a_4\\0&1&0&0\\0&0&1&d_5\\0&0&0&1\end{bmatrix};\quad
{}^{5}_{6}T=\begin{bmatrix}0&-1&0&0\\0&0&-1&0\\1&0&0&0\\0&0&0&1\end{bmatrix};
$$

$$
{}^{6}_{7}T=\begin{bmatrix}1&0&0&a_6\\0&1&0&0\\0&0&1&0\\0&0&0&1\end{bmatrix}
$$

$$
{}^{0}_{7}T={}^{0}_{1}T\ {}^{1}_{2}T\ {}^{2}_{3}T\ {}^{3}_{4}T\ {}^{4}_{5}T\ {}^{5}_{6}T\ {}^{6}_{7}T \tag{6}
$$

The parallel part of the SILS robot is that the two moving joints in the vertical moving mechanism drive the rods to complete the telescopic motion along the axis of the endoscope, and the vertical moving joints drive the two connecting rods to move. The two rods and the lead screw form a triangle shape. The geometric relationship can be obtained in (7) and (8). By substituting the results obtained from the parallel part into the series part, the relative position and pose changes of the SILS robot can be obtained.

$$
\cos\beta=\frac{l^2+d_3^2-b^2}{2\,d_3\,l} \tag{7}
$$

$$
\left.\begin{aligned}Z_B&=l\sin\beta\\X_B&=l\cos\beta\end{aligned}\right\} \tag{8}
$$

$$
\begin{bmatrix}p_x\\p_y\\p_z\\1\end{bmatrix}=\begin{bmatrix}l\sin\beta+a_4\ c_4\\d_2+d_3+a_4\ c_4\\l\cos\beta+a_6+d_1+d_5\\1\end{bmatrix} \tag{9}
$$

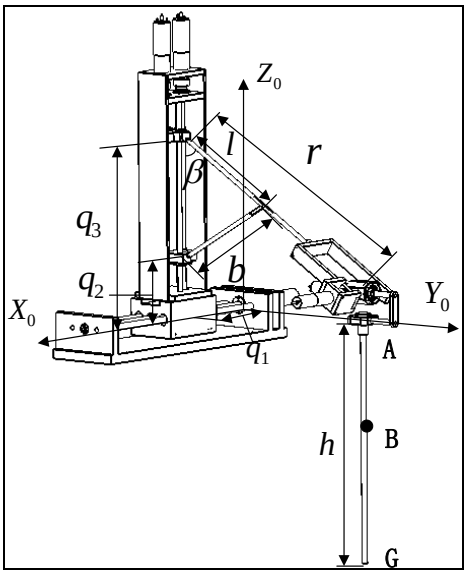

Figure 5 Robot system model

B. Inverse kinematics and Jacobian matrix

The coordinate system of the proposed single-incision laparoscopic surgical robot is defined, as shown in Figure 5. The one end of the horizontal movement mechanism of the robot positioning mechanism is the base coordinate system (X_0, Y_0, Z_0). The moving distance of the sliding table in the horizontal moving mechanism is defined as q_1, and the moving distance of the sliding block in the vertical moving mechanism is defined as q_2 and q_3, respectively. The endoscope rotation angles driven by the motor in the position and pose adjustment mechanism are q_4 and q_5, respectively. According to the analysis of the parameters of the previous design, the length $r$of the first link, the length b of the second link, the length l between the hinge of the first and second link and the first sliding block of the vertical movement mechanism, and the length h of the endoscope are already known. β is the angle between connecting rod and vertical direction. The end effector coordinate system is defined as shown in Figure 6. Since the position of the end effector endoscope in the abdominal cavity changes momentarily, The coordinate system (X_A, Y_A, Z_A), (X_B, Y_B, Z_B) and (X_G, Y_G, Z_G) of the rotating center point A, incision point B and end point G were established, and (X_A', Y_A', Z_A') is the translation coordinate system of (X_A, Y_A, Z_A) at point B. The rotation angle φ and the endoscope inclination

angle θ in the abdominal cavity are indicated in Figure 6. The distance from endoscope's point B along the incision to the end point G is defined as h_1. According to the defined coordinate system and its known values, the rest variables are derived using the coordinates of the end effector. The final result is the inverse solution of the robot kinematics.

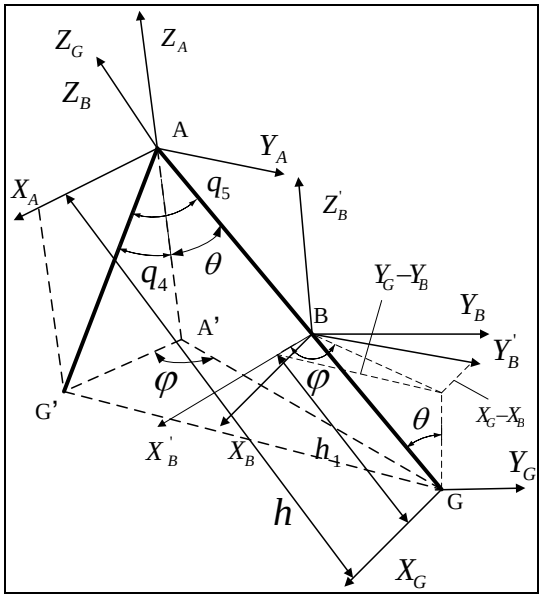

Figure 6 End effector coordinate system

It can be derived from Figure 5 and Figure 6 that the generalized motion factors q_1, q_2, q_3, q_4, q_5 are known, as well as the geometric parameters b, h, l, and r. Thus, the coordinates of point A can be directly written:

$$\left.\begin{aligned} X_A &= q_1 \\ Y_A &= r\cos\beta \\ Z_A &= q_3 - r\sin\beta \end{aligned}\right\} \quad (10)$$

where

$$\cos\beta = \frac{(q_3-q_2)^2 + l^2 - b^2}{2(q_3-q_2)l}$$

$$\sin\beta = 1 - \left(\frac{(q_3-q_2)^2 + l^2 - b^2}{2(q_3-q_2)l}\right)^2$$

According to the point A coordinates, the coordinate value of point G and the angle of φ and θ can be obtained.

$$\left.\begin{aligned} X_G &= X_A - h\sqrt{2(1-\cos q_5)} \\ Y_G &= Y_A + h\sin q_4 \\ Z_G &= Z_A - h\cos q_4 \\ \varphi &= \arctan\left(\frac{Y_A - Y_G}{X_A - X_G}\right) \\ \theta &= \arctan\left(\frac{\sqrt{(X_A-X_G)^2 + (Y_A-Y_G)^2}}{Z_A - Z_G}\right) \end{aligned}\right\} \quad (11)$$

Based on the established geometric model, the kinematic equation is obtained. The implicit equation for the end of the abdominal surgical robot is defined as follows:

$$\left.\begin{aligned} f_1(q_1, X_G, \varphi, \theta) &= X_G - h\sin\theta\cos\varphi - q_1 = 0 \\ f_2(q_2, q_3 Y_G, \varphi, \theta) &= Y_G - h\sin\theta\sin\varphi - r\sin\beta = 0 \\ f_3(q_2, q_3, Z_G, \theta) &= Z_G + h\cos\theta - q_3 + r\cos\beta = 0 \\ f_4(q_4, \varphi, \theta) &= \sin\theta\sin\varphi\cos q_4 - \sin q_4\cos\theta = 0 \\ f_5(q_5, \varphi, \theta) &= \sin^2\varphi\sin^2\theta - \sin^2\theta + 1 - \cos^2 q_5 = 0 \end{aligned}\right\} \quad (12)$$

The kinematics model can be represented by a matrix:

$$A\dot{X} + B\dot{q} = 0 \quad (13)$$

According to the formula of the kinematic model obtained, $\dot{q} = [\dot{q}_1, \dot{q}_2, \dot{q}_3, \dot{q}_4, \dot{q}_5]^{\mathrm{T}}$ reflects the tiny motion of joint space, and $\dot{X} = [\dot{X}_G, \dot{Y}_G, \dot{Z}_G, \dot{\varphi}, \dot{\theta}]$ reflects the slight motion of the operating space. The slight motion of the operating space consists of slight line displacements and slight angular displacements of the joint space, so the kinematic model can be rewritten as:

$$\dot{X} = -A^{-1}B\dot{q} \quad (14)$$

According to (14), the robot's velocity Jacobian can be obtained:

$$J = -A^{-1}B \quad (15)$$

IV. Dynamic Modeling of Laparoscopic Surgical Robot

A. Kane method

The single-incision laparoscopic surgical robot is a hybrid robot, which can to be divided into several parts according to its structural characteristics for dynamic analysis. In this paper, the Kane method is used to establish the dynamic equations of robot's components where the dynamic equations of several components can then be combined. The equation can be interpreted as the statement that the sum of the generalized active force F_γ and the generalized inertial force F_γ^* corresponding to the γ-th independent velocity of the system is zero.

$$F_\gamma + F_\gamma^* = 0 \quad (16)$$

The generalized active force is defined as:

$$F_\gamma = R_\gamma \cdot u_\gamma' + L_\gamma \cdot \omega_\gamma' \quad (17)$$

where F_γ is the principal vector of the centroid of the rigid body, L_γ is the principal moment of the centroid, u_γ' is the partial velocity at which the centroid corresponds to an independent velocity, and ω_γ' is the partial.

The generalized inertial force is defined as:

$$F_\gamma^* = R_\gamma^* \cdot u_\gamma' + L_\gamma^* \cdot \omega_\gamma' \quad (18)$$

where R_γ^* is the principal vector of inertia of the centric of the rigid body, L_γ^* is the principal moment of inertia of the centric,

u'_γ is the partial velocity at which the centric corresponds to an independent velocity, and ω'_γ is the partial. The principal inertia vector can be obtained according to Newton's second law, and the inertia principal moment can be obtained according to the inertial tensor.

B. Robot horizontal moving mechanism

Assuming that the generalized coordinate of the horizontal movement mechanism of the robot is q_1, the generalized velocity is $u_1 = \dot{q}_1$. Therefore, for the sliding table with the screw nut pair, the velocity is defined as $V_h = [G_v^H]\dot{q}_1$, thus the partial velocity of the slide is $u'_h = [G_v^H]$. Where $[G_v^H]$ is the first-order influence coefficient, which corresponds to the first column of the velocity Jacobian matrix in robot modeling. The sliding table has only a linear motion in the horizontal moving mechanism, so the angular velocity is $\omega_h = 0$, and the partial angular velocity is $\omega'_h = 0$. The mass of the horizontal moving mechanism is M_1, and the generalized active force caused by the volume force is:

$$F_{TG(1)} = M_1\, g\, u'_h \tag{19}$$

The generalized active force caused by the driving force is mainly provided by the motor, so the generalized active force is f_1.

$$F_{r(1)} = F_{TG(1)} + f_1 \tag{20}$$

According to the calculation formula of the generalized inertial force, the principal vector of the inertial force R^*_γ is required. Since the mechanism does not produce angular velocities, it is not necessary to obtain the principal moment L^*_γ. According to Newton's second law formula, the principal vector of inertial force can be obtained by $R^*_\gamma = -M_1 a$. The acceleration a can be derived from the generalized velocity:

$$a_1 = \dot{q}_1^T \left[H_v^H\right]\dot{q}_1 + \left[G_v^H\right]\ddot{q}_1 \tag{21}$$

where $[H_v^H]$ is the second-order influence coefficient, which corresponds to the first column of the acceleration Jacobian matrix in robot research.

In summary, the generalized inertial force of the robot horizontal moving mechanism is:

$$F^*_{r(1)} = -M_1\left(\dot{q}_1^T \left[H_v^H\right]\dot{q}_1 + \left[G_v^H\right]\ddot{q}_1\right)u'_h \tag{22}$$

The generalized active force and the generalized inertial force of the horizontal moving mechanism are substituted into (16), and the driving force of the robot horizontal moving mechanism is obtained as follows:

$$f_1 = M_1\left(\dot{q}_1^T \left[H_v^H\right]\dot{q}_1 + \left[G_v^H\right]\ddot{q}_1\right)u'_h - M_1 g u'_h \tag{23}$$

C. Robot vertical moving mechanism

The generalized coordinates of the vertical moving parallel mechanism are assumed to be q_2 and q_3, with its generalized velocity being $u_2 = \dot{q}_2$, $u_3 = \dot{q}_3$. According to the definition of the partial velocity, its partial velocity is being $V_{H(r)} = [G_v^H]$, where the $[G_v^H]$ is the first-order influence coefficient, corresponding to the second and third columns in the velocity Jacobian matrix. The generalized driving force caused by the volume force includes the volume force of the link and the volume force of the sliding table, with the volume force of the link calculated by:

$$F_{g(r)} = g\sum_{i=1}^{2} m_i V_{g(r)} \tag{24}$$

Since the sliding table's volume force considers only the gravity effect its volume force can be obtained by:

$$F_{L(r)} = g\sum_{i=1}^{2} m_{Li} V_{H(r)} \tag{25}$$

The generalized active force caused by the driving force is mainly caused by the two motors in the vertical moving mechanism, with each value being equal to $F_Q = [f_2\ f_3]$.

In summary, the generalized active force of the vertical moving robot's mechanism is as follows:

$$F_{r(2)} = F_{g(r)} + F_{L(r)} + F_Q \tag{26}$$

The second order influence coefficient correspond to the second and third columns of the acceleration Jacobian matrix, thus the inertial force principal vector of the link is:

$$R^*_{g(r)} = m_i\left(\dot{q}_i^T \left[H_v^H\right]\dot{q}_i + \left[G_v^H\right]\ddot{q}_i\right),\ \ i = 2, 3 \tag{27}$$

The inertial force principal vector of the sliding table is:

$$R^*_{L(r)} = m_{Li}\left(\dot{q}_i^T \left[H_v^H\right]\dot{q}_i + \left[G_v^H\right]\ddot{q}_i\right),\ i = 2, 3 \tag{28}$$

The principal rotational inertial force is equal to $L_i = -I_i\varepsilon_i - \omega_i \times I_i\omega_i$ .The main rotational inertial force can be produced by the link of the parallel mechanism, which can be calculated according to the rotational inertia formula of a homogeneous body: $J_{Ci} = (m_i l_i^2)/3$,where m_i is the mass of the link and l_i is the length of the link.

In summary, the generalized inertial force of the parallel mechanism is:

$$F^*_{r(2)} = -\left(R^*_{g(r)} V_{g(r)} + R^*_{L(r)} V_{H(r)} + J_{Ci}\omega_{i(r)}\right) \tag{29}$$

According to the definition of Kane equation, the generalized active force and the generalized inertial force of the vertical moving mechanism are substituted into (16), with the driving force of the vertical moving mechanism of the robot calculated as follows:

$$\begin{aligned} f_2 = {} & m_1\, a_2\, V_{g(1)} + m_{L1}\, a_2\, V_{H(1)} + J_{C1}\, \omega_{11} \\ & + J_{C1}\, \omega_{12} - m_1\, g\, V_{g(1)} - m_2\, g\, V_{g(1)} - m_{L1}\, g\, V_{H(1)} \end{aligned} \tag{30}$$

$$\begin{aligned} f_3 = {} & m_2\, a_3\, V_{g(2)} + m_{L2}\, a_3\, V_{H(2)} + J_{C2}\, \omega_{21} \\ & + J_{C2}\, \omega_{22} - m_1\, g\, V_{g(2)} - m_2\, g\, V_{g(2)} - m_{L2}\, g\, V_{H(2)} \end{aligned} \tag{31}$$

D. Robot position and pose adjustment mechanism

The two revolute pairs of position and pose adjustment mechanism that generate the rotation angle are the revolute pairs A and B whose rotation axes are perpendicular to each other, so the generalized coordinates are assumed to be X_G, Y_G, Z_G, α_1, α_2, and the generalized rate is $u_1 = \dot{X}_G$, $u_2 = \dot{Y}_G$, $u_3 = \dot{Z}_G$, $u_4 = \dot{\alpha}_1$, $u_5 = \dot{\alpha}_2$. The angular velocity of the revolute pair A is equal to $\omega_A = \dot{\alpha}_1 e_1 = e_1 u_4$. The partial angular velocity of the revolute pair A is: $\omega_{A(4)} = e_1 = \cos q_4$, $\omega_{A(1)} = \omega_{A(2)} = \omega_{A(3)} = \omega_{A(5)} = 0$ (where q_4 is the angle at which the endoscope is adjusted). The angular velocity of the revolute pair B is: $\omega_B = \omega_A + {}^A\omega_B = \dot{\alpha}_1 e_2 + \dot{\alpha}_2 e_2 = e_1 u_4 + e_2 u_5$, where ${}^A\omega_B$ is the angular velocity of the revolute pair B with respect to revolute pair A. Therefore, the partial angular velocity of the revolute pair B is $\omega_{B(4)} = e_1 = \cos q_4$, $\omega_{B(5)} = e_2 = (\sin q_5)/(\sin q_4)$, $\omega_{B(1)} = \omega_{B(2)} = \omega_{B(3)} = 0$.

The generalized active force caused by the driving torque is mainly produced by the two motors in the position and pose adjustment mechanism, where $F = [\tau_4\ \tau_5]$. The force and moment generated by the end effector and the working area can berespectively simplified to R_C and L_C on the endoscope. Since the endoscope has no moving velocity, the generalized active force caused by the contact force of the end effector is: $F_{Ci} = L_{Ci}\omega_{B(r)}$, where $L_{Ci} = m_i g l_i$.

In summary, the generalized active force of the position and pose adjustment mechanism is:

$$F_r = F_J + F_{Ci} \tag{32}$$

According to Eq.18, the principal moment of inertia of the revolute pair A is: $L_A^* = J_{c1} = (m_1 R^2/2) + (m_2 l^2/3)$, with the principal moment of inertia of the revolute pair B being equal to $L_B^* = J_{c2} = m_2 l^2/3$, where m_1 is the mass of the shaft, R is the radius of the shaft, m_2 the mass of the endoscope, and l the length of the endoscope.

According to the above analysis, the generalized inertial force of the position and pose adjustment mechanism is:

$$F_{r(i)}^* = -J_{ci}\ \omega_{i(r)} \tag{33}$$

Finally, based on the Kane equation definition, the generalized active force and the generalized inertial force of the position and pose adjustment mechanism are substituted into (16), and the driving torque of the position and pose adjustment mechanism of the robot is obtained as follows:

$$\tau_4 = J_{c1}\ \omega_{A(4)} - L_{C1}\ \omega_{B(4)} \tag{34}$$

$$\tau_5 = J_{c2}\ \omega_{B(5)} - L_{C2}\ \omega_{B(5)} \tag{35}$$

E. Kane dynamics equation

By combining the above driving force and driving torque equation, the Kane dynamic equation of the single-incision laparoscopic surgical robot can be obtained by:

$$f_1 = M_1\ a_1\ u_h^{'} - M_1\ g\ u_h^{'} \tag{36}$$

$$f_2 = m_1\ a_2\ V_{g(1)} + m_{L1}\ a_2\ V_{H(1)} + J_{C1}\ \omega_{11} + J_{C1}\ \omega_{12} - m_1\ g\ V_{g(1)} - m_2\ g\ V_{g(1)} - m_{L1}\ g\ V_{H(1)} \tag{37}$$

$$f_3 = m_2\ a_3\ V_{g(2)} + m_{L2}\ a_3\ V_{H(2)} + J_{C2}\ \omega_{21} + J_{C2}\ \omega_{22} - m_2\ g\ V_{g(2)} - m_2\ g\ V_{g(2)} - m_{L2}\ g\ V_{H(2)} \tag{38}$$

$$\tau_4 = J_{c1}\ \omega_{A(4)} - L_C\ \omega_{B(4)} \tag{39}$$

$$\tau_5 = J_{c2}\ \omega_{B(5)} - L_C\ \omega_{B(5)} \tag{40}$$

V. Kinematics Simulation of Laparoscopic Surgical Robot

The displacement, velocity and acceleration of each active joint of the robot are known. Based on kinematics model and Jacobian matrix, numerical simulation is carried out by using MATLAB software. The displacement, velocity and acceleration of the endoscope end point in the basic coordinate system are calculated, so as to verify the correctness of kinematics equation.The values of each active joint of the SILS robot are set as follows:

Initial position and termination position of q_{1i} : $q_{1i} = 120\ mm$; $q_{1f} = 180\ mm$.

Initial position and termination position of q_2 : $q_{2i} = 120\ mm$; $q_{2f} = 180\ mm$.

Initial position and termination position of q_3 : $q_{3i} = 260\ mm$; $q_{3f} = 320\ mm$.

Initial position and termination position of q_4 : $q_{4i} = 0$; $q_{4f} = 30°$.

Initial position and termination position of q_5 : $q_{5i} = 0$; $q_{5f} = 30°$.

Assuming that the motion parameters of the moving joint in each active joint of the robot are set as follows:

$v_{\max} = 10$ mm/s, $a_{\max} = 5$ mm/s^2, $\omega_{\max} = 4$ rad/s, and $\alpha_{\max} = 2$ rad/s^2. The motion simulation results of endoscope end point in workspace are shown in Figure 7.

If the motion of the endoscope end point is known, the displacement, velocity and acceleration of each active joint of the robot can be deduced according to the kinematics model. The parameter values of the endoscope end point of the robot are set as follows:

- Initial position and termination position of X_G: $X_{Gi} = 120\ mm$, $X_{Gf} = -37.91\ mm$.
- Initial position and termination position of Y_G: $Y_{Gi} = 150\ mm$, $Y_{Gf} = -402.2\ mm$.

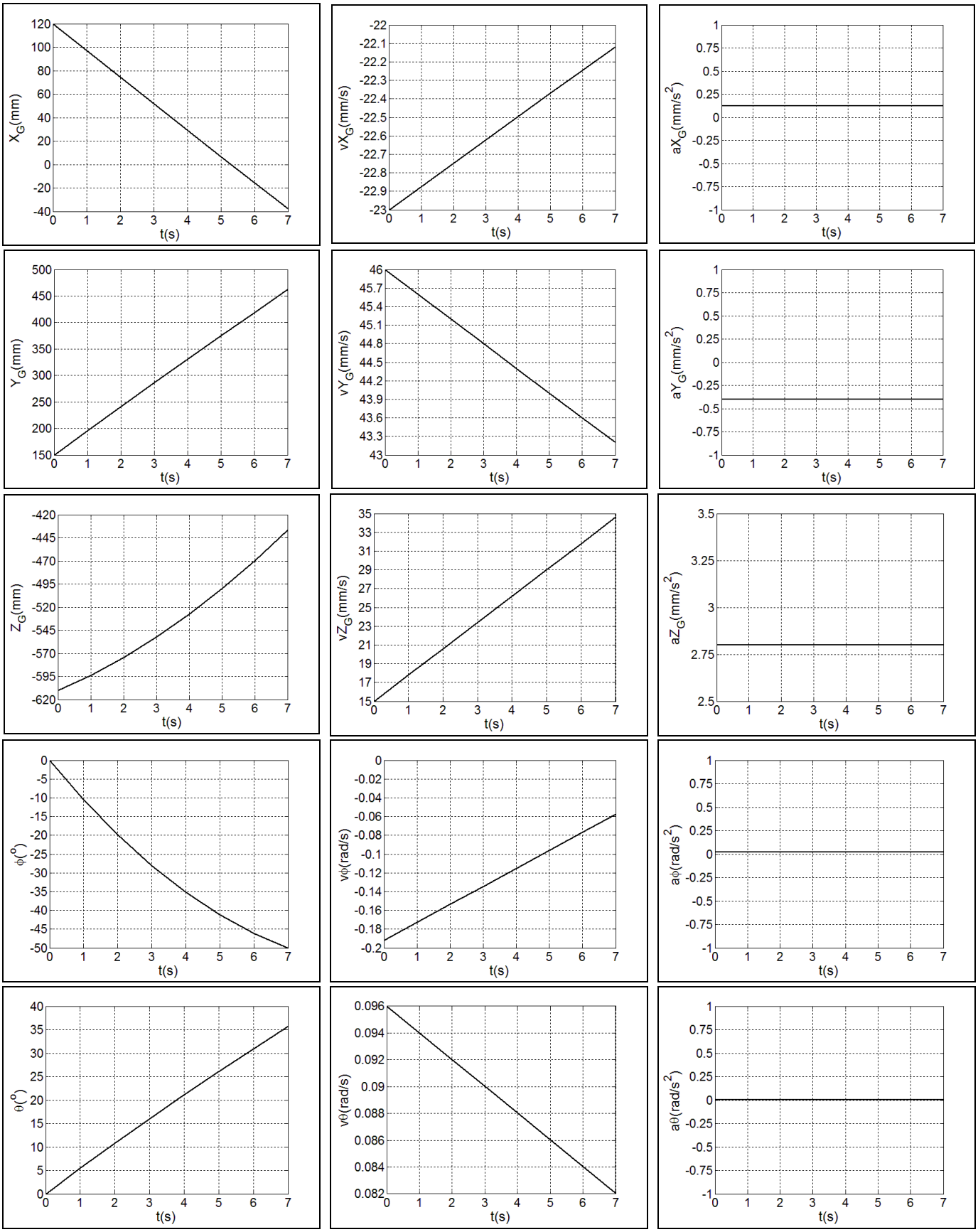

Figure 7 The motion simulation of the endoscope endpoint

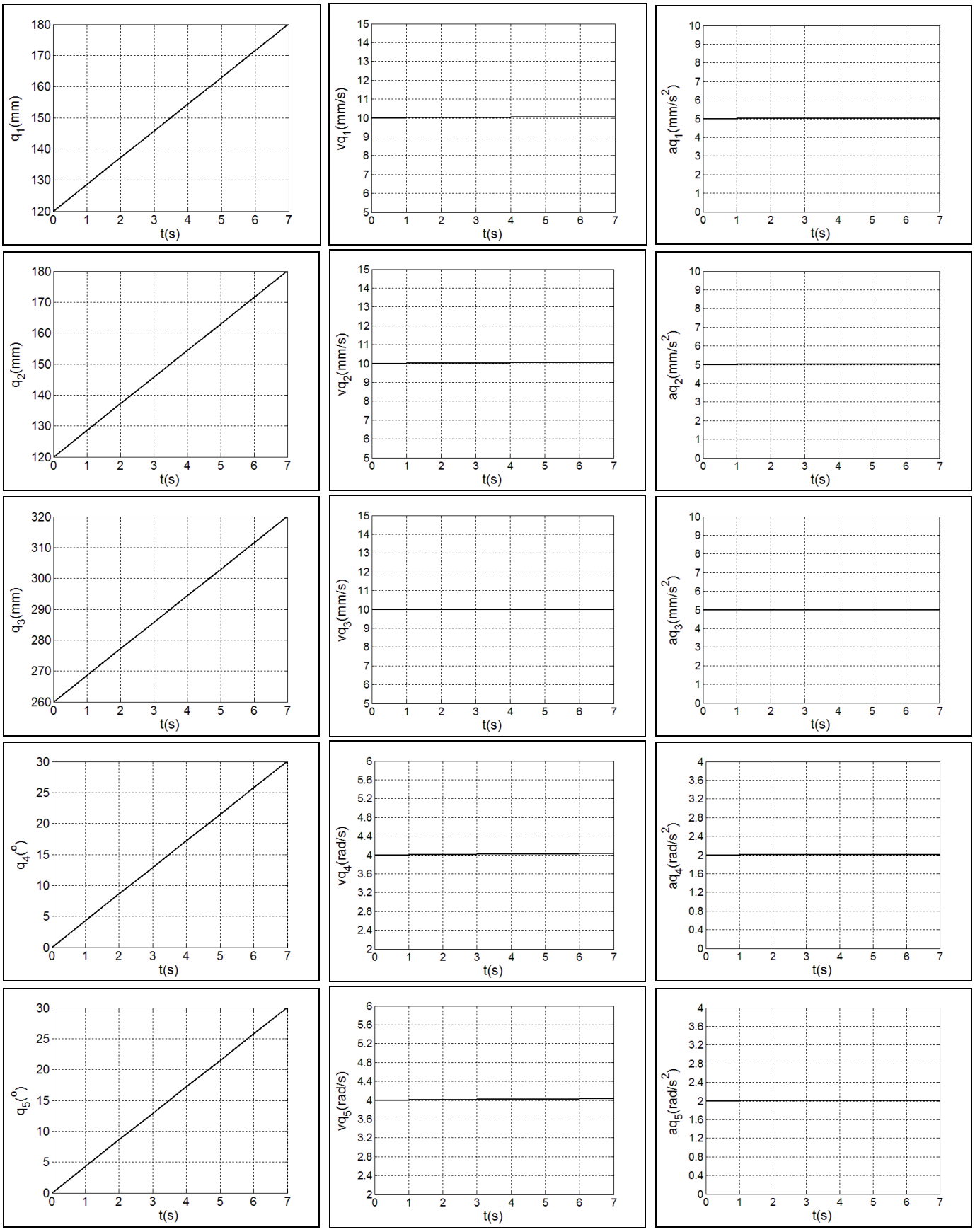

Figure 8 The motion simulation of the SILS robot's active joint

- Initial position and termination position of Z_G: $Z_{Gi} = -610\ mm, Z_{Gf} = -436.4\ mm$.
- Initial position and termination position of φ: $\varphi_i = 0, \varphi_f = -49.8°$.
- Initial position and termination position of θ: $\theta_i = 0, \theta_f = 35.71°$.
- Initial velocity, termination velocity, and acceleration of X_G: $v_{xi} = -23\ \text{mm/s}, v_{xf} = -22.118\ \text{mm/s}, a_x = 0.126\ \text{mm/s}^2$.
- Initial velocity, termination velocity and acceleration of Y_G: $v_{yi} = 46\ \text{mm/s}, v_{yf} = 43.2\ \text{mm/s}, a_y = 0.4\ \text{mm/s}^2$.
- Initial velocity, termination velocity and acceleration of Z_G: $v_{zi} = 15\ \text{mm/s}, v_{zf} = 34.6\ \text{mm/s}, a_z = 2.8\ \text{mm/s}^2$.
- Initial velocity, termination velocity and acceleration of φ: $v_{\varphi i} = -0.192\ \text{rad/s}, v_{\varphi f} = -0.0576\ \text{rad/s}, a_\varphi = 0.0192\ \text{rad/s}^2$.
- Initial velocity, termination velocity and acceleration of θ: $v_{\theta i} = 0.096\ \text{rad/s}, v_{\theta f} = 0.0821\ \text{rad/s}, a_\theta = 0.002\ \text{rad/s}^2$.

By substituting the set parameters into the inverse kinematics model, the motion of each active joint of the robot is obtained as shown in Figure 8.

According to the simulation results of forward and inverse kinematics, when the active joint of the SILS robot is set as a uniformly accelerated motion, the motion parameters of the end effector are also a uniformly accelerated motion mode. At the same time, the motion parameters of the active joint calculated by the inverse kinematics model are in accordance with the initial motion parameters, which prove the correctness of the kinematic model of the SILS robot.

VI. Dynamics Simulation of Laparoscopic Surgical Robot

In order to facilitate a numerical simulation analysis, the robot's motion time range is set to $0\sim15s$.The robot mechanism motion can be divided into two kinds of motion situations for dynamic numerical simulation: sequential motion and simultaneous motion.

(1) Sequential motion of robot mechanism

Within $0\sim5s$, the horizontal moving mechanism sliding table in the robot positioning mechanism performs a uniform acceleration motion in the horizontal direction, and the equation of motion is set for $s = 4.8t^2$. Within $5s\sim10s$, the upper and lower sliding blocks of the vertical moving mechanism in the robot positioning mechanism perform a uniform acceleration motion, and the equation of motion is set for $s = 4.8t^2$. The sliding blocks drive the position and pose adjustment mechanism to move through the links. Within $10s\sim15s$, the motor adjusts the final posture of the endoscope in the end effector in the position and pose adjustment mechanism. Within $10s\sim13s$, the motor in which the axis is collinear with the X-axis in the position and pose adjustment mechanism accelerates and rotates with the equation of motion being $s = 12.89t^2$. Within $13s\sim15s$, the motor in which the axis is collinear with the Y-axis in the position and pose adjustment mechanism accelerates and rotates with the equivalent motion equation being $s = 5.73t^2$. When the robot mechanism moves in time series, the end of the endoscope forms four motion trajectories in space as follows:

The first trajectory is a line segment whose motion trajectory equation is:

$$\left.\begin{aligned} x &= 24t \\ y &= 0 \\ z &= 0 \end{aligned}\right\} \quad (41)$$

The second trajectory is an arc whose motion trajectory equation is:

$$\left.\begin{aligned} (x-120)^2+(y-395)^2+(z-924)^2 &= 618^2 \\ x &= 120 \\ 0 \le y &< 280 \\ 0 \le z &< 190 \end{aligned}\right\} \quad (42)$$

The third trajectory is an arc whose motion trajectory equation is:

$$\left.\begin{aligned} (x-120)^2+(y-47)^2+(z-164)^2 &= 500^2 \\ x &= 120 \\ 280 \le y &< 450 \\ 190 \le z &< 290 \end{aligned}\right\} \quad (43)$$

The fourth trajectory is an arc whose motion trajectory equation is:

$$\left.\begin{aligned} (x-120)^2+(y-47)^2+(z-164)^2 &= 500^2 \\ -0.135x - z + 300 &= 0 \\ -80 \le x &\le 120 \\ 434 < y &\le 450 \\ 290 \le z &\le 320 \end{aligned}\right\} \quad (44)$$

Individual part mass is known, where the mass of the horizontal sliding table is 3.002 kg, the mass of the sliding block in the vertical moving mechanism is 0.162 kg, the mass of the first link is 0.052 kg, the mass of the second link is 0.033 kg,the mass of the position and pose adjustment frame is 0.012 kg, and the mass of the cross seat is 0.187 kg.The mass parameters of the relevant mechanisms were substituted into the dynamic equations, and the numerical diagram of the driving force (torque) of each mechanism of the robot sequential motion is shown in Figure 9 which was obtained by numerical analysis using MATLAB7.0 software.

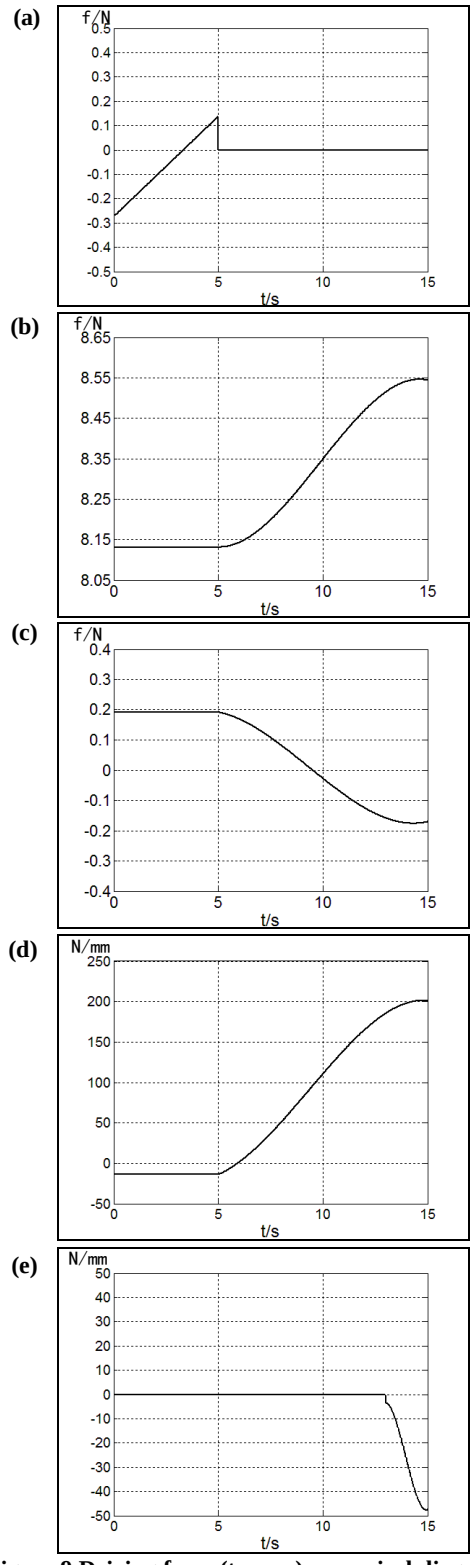

Figure 9 Driving force (torque) numerical diagrams of mechanisms of robot sequential motion, including:
(a) Horizontal moving mechanism driving force f1
(b)Vertical moving mechanism driving force f2,
(c)Vertical moving mechanism driving force f3,
(d) Position and pose adjustment mechanism driving torque τ4,
(e) Position and pose adjustment mechanism driving torque τ5

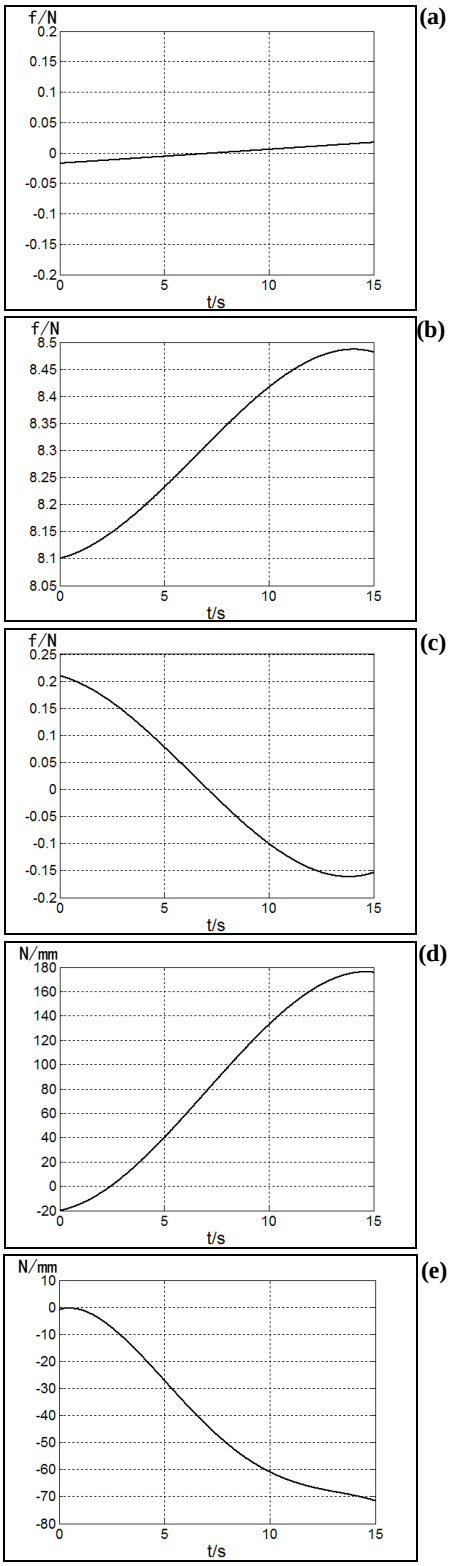

Figure 10 Driving force (torque) numerical diagram for mechanisms of robot simultaneous motion, including
a) Horizontal moving mechanism driving forcef1,
b)Vertical moving mechanism driving force f2,
c)Vertical moving mechanism driving force f3,
d) Position and pose adjustment mechanism driving torque τ4,
e) Position and pose adjustment mechanism driving torque τ5

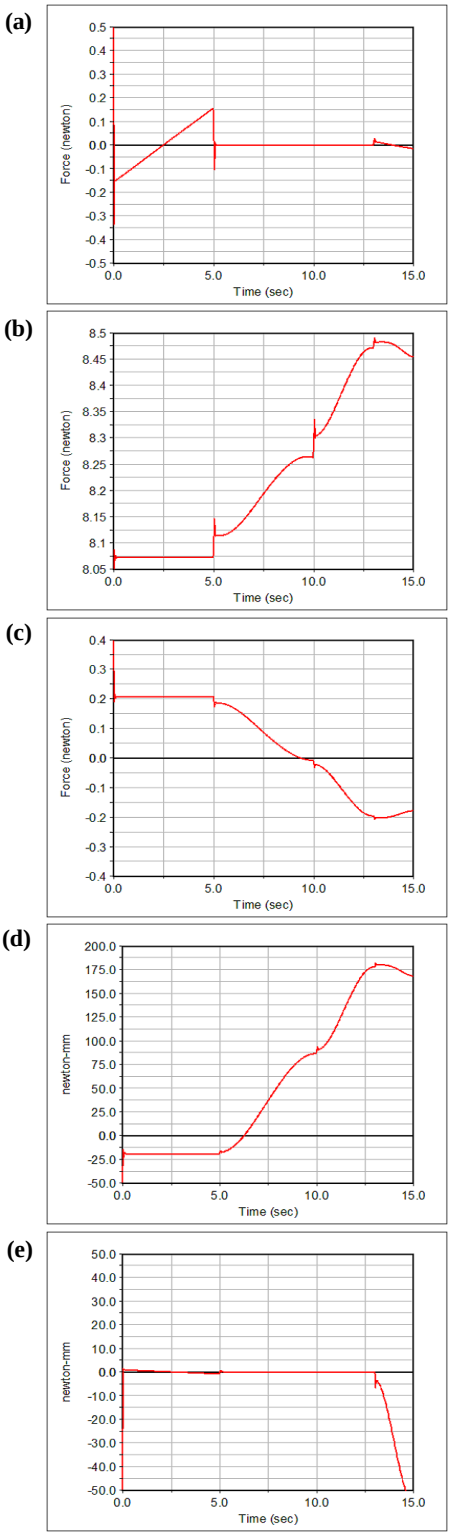

Figure 11 Simulation of driving force (torque) of robot mechanism in control group, including
a) Horizontal moving mechanism driving force f1,
b) Vertical moving mechanism driving force f2,
c) Vertical movement mechanism driving force f3,
d) Position and pose adjustment mechanism driving torqueτ4,
e) Position and pose adjustment mechanism driving torqueτ5.

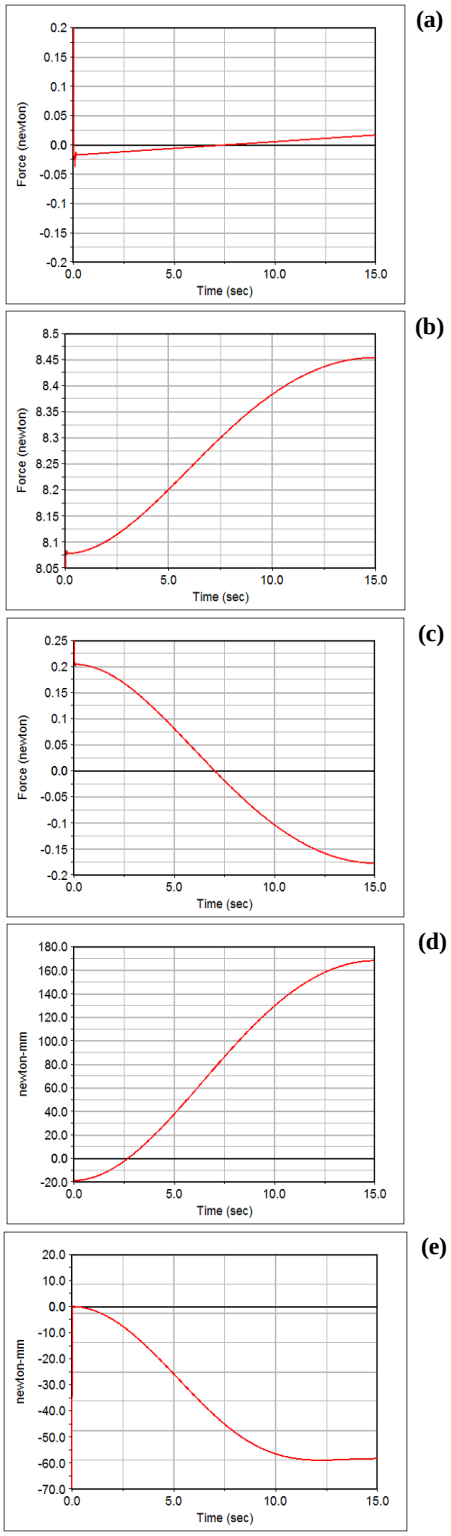

Figure 12 Simulation of driving force (torque) of robot mechanism in control group, including
a) Horizontal moving mechanism driving force f1,
b) Vertical moving mechanism driving force f2,
c) Vertical movement mechanism driving force f3,
d) Position and pose adjustment mechanism driving torqueτ4,
e) Position and pose adjustment mechanism driving torqueτ5.

(2) Simultaneous motion of robot mechanism

Within $0\sim15s$, the horizontal moving mechanism and the vertical moving mechanism in the single-incision laparoscopic surgical robot perform the uniform acceleration linear motion, and the equation of motion is set for $s = 0.9375t^2$. During $0\sim15s$, the endoscopic position and pose adjustment mechanism of the single-incision laparoscopic surgical robot performs a uniform acceleration rotation motion described as $s = 322.29t^2$.The motion trajectory equation is:

$$\left.\begin{aligned}(x-347)^2+(y-800)^2+(z-286)^2 &= 715^2\\ 0.0105y+0.0122z+1.249 &= 0\\ 0\le x<320\\ 0\le y<440\\ -315<z\le 0\end{aligned}\right\} \quad (45)$$

According to the defined motion trajectory of the simultaneous motion of the robot mechanisms, a numerical simulation is carried out, with the numerical diagram of the driving force (torque) for each robot's mechanism shown in Figure 10.

A virtual prototype platform of the single-incision laparoscopic surgical robot is established, including all the necessary parameters and movement plans of the robot mechanism. The robot mechanisms can move in sequence, dividing the route of the endoscope movement into a series of independent movements. The time sequence of the movement of the robot mechanism is estimated by the amount of change in the analysis experiment, meaning that the moving time of the robot mechanism is a variable, while the movement distance and the angle parameter of the robot mechanism are taken as a reference. In the control group, each robot mechanism moves in a sequence. In the experimental group, robot mechanisms move at the same time.

The movement duration of the single-incision laparoscopic robot is between $0\sim15s$. By using the virtual simulation software ADAMS to set the time sequence movement, the simulation image of each driving force (torque) of the robot mechanism of the control group can be obtained, as shown in Figure 11.

Based on the movement of the robot in the actual work, we accordingly change the movement plan of the mechanism. We set the movement time range of the robot to $0\sim15s$, and use the ADAMS virtual simulation software to set the movement of the robot. Each mechanism in the robot moves at the same time within this time range obtaining the simulation image of each driving force (torque) of the experimental group robot, as shown in Figure 12.

According to the numerical simulation results of Figure 9 and Figure 10 and the virtual simulation results of Figure 11 and Figure 12, it can be noted that the theoretical calculation results are consistent with the virtual simulation results. Furthermore, the correctness of the robot dynamic simulation is verified, and the theoretical basis for the dynamic stiffness analysis of the robot is established.

VII. Dynamic Stiffness Analysis of Laparoscopic Surgical Robot

Through stiffness analysis, the stiffness performance of the robot in the operating space is evaluated [29]. Higher stiffness can ensure that the deformation of the robot is smaller in the working process [30]. Because the surgical robot is composed of many parts and components in different ways of connection and motion, the deformation of the robot is quite complex after being stressed, including elastic deformation, plastic deformation, gap and friction. However, by using the virtual work's principles, the coupling relationship between the force Jacobian matrix and the velocity Jacobian matrix can be obtained, while the stiffness matrix of the mechanism can be established. Considering the external force acting on the mechanism, the dynamic stiffness matrix model of the conservation transformation of the single-incision laparoscopic robot mechanism is determined as follows:

$$K_d = \left[\frac{\partial J^T}{\partial q_1} f_1, \frac{\partial J^T}{\partial q_2} f_2, \frac{\partial J^T}{\partial q_3} f_3, \frac{\partial J^T}{\partial q_4}\tau_4, \frac{\partial J^T}{\partial q_5}\tau_5\right] \quad (46)$$

In order to evaluate the distribution of the stiffness of the robot mechanisms in different position and posture, it is necessary to use the Rayleigh quotient of the stiffness matrix. The stiffness, which is defined as the ratio of the square of the external force vector module acting on the end effector of the mechanism to the square of its deformation vector module, is calculated as follows:

$$\|F\|_2 = \sqrt{R(\delta X)}\,\|\delta X\|_2 \quad (47)$$

where δX is the generalized joint pose variable and F is the generalized joint moment.

According to the above formula, the eigenvalues λ_i $(i = 1,2,\cdots,5)$ of the matrix $K_d^T K_d$ have a certain relationship: $\lambda_1 \le \lambda_2 \le \lambda_3 \le \lambda_4 \le \lambda_5$, where for any possible non-zero δX, there will be $\lambda_1 \le R(\delta X) \le \lambda_5$. Therefore, after applying a certain load on the end effector, if $\sqrt{R(\delta X)}$ is larger, the deformation δX of the mechanism will be smaller, indicating that the stiffness is higher. Therefore, the stiffness at each point can be evaluated according to the square root of the minimum eigenvalue of the matrix $K_d^T K_d$, that is, the minimum singular value of the static stiffness matrix of the robot, allowing the overall evaluation of the stiffness performance. According to the above analysis, the maximum deformation is defined as follows:

$$S = \sqrt{R(\delta X)} = \sqrt{\min(\lambda_1,\lambda_2,\ldots,\lambda_5)} \quad (48)$$

where S is the maximum deformation and $\min(\lambda_1,\lambda_2,\cdots,\lambda_5)$ is the minimum eigenvalue of matrix $K_d^T K_d$.

With the relevant parameters in the stiffness model of the laparoscopic robot being selected, the effect of each joint variable on overall stiffness can be shown in Fig.13 and 14. According to the effect of the joint deformation on the maximum deformation distribution of overall stiffness, each joint variable introduce different effects in the overall stiffness. This is apparent in the simulation image of the maximum deformation of the mechanism under the above two modes of motion where the mechanisms under the sequential motion

present a large deformation in the early stage of the robot movement. As the various mechanisms of the robot complete the corresponding movement, a small deformation is apparent but proves that the mechanisms are suitable for the robot movement.The mechanisms under the simultaneous motion have a small deformation, which can ensure the dynamic stability of the robot mechanisms during the movement, thus the precise operation of the laparoscopic surgery can be ensured.

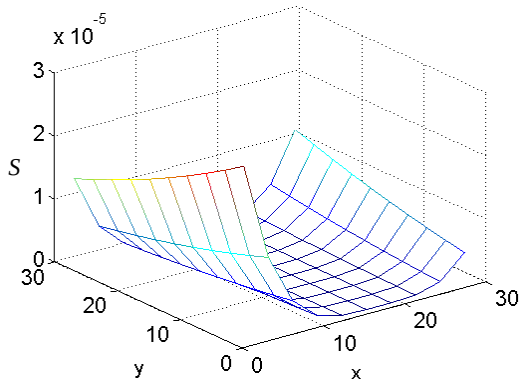

Figure 13 Maximum deformation of sequential motion

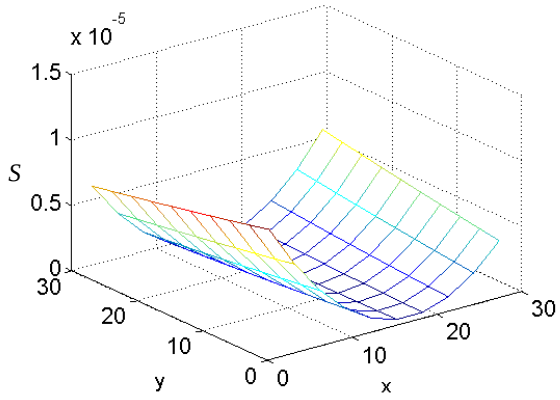

Figure 14 Maximum deformation of simultaneous motion

VIII. CONCLUSIONS

This paper proposed a 5-DOF-single-incision laparoscopic surgical robot with serial-hybrid mixing. The inverse kinematics equation and Jacobian matrix of the robot are derived by D-H method and geometric method with its dynamic equation determined by Kane method. Extensive numerical and virtual simulations of the robot kinematics and dynamics equation were carried out verifying the correctness of the established kinematics and dynamic model of the surgical robot, and establishing a theoretical basis for the performance optimization and dynamic control of the proposed surgical robot. Finally, the dynamic stiffness model is analyzed and evaluated and the evaluation index of the robot was also defined based on the dynamic model of the robot.

ACKNOWLEDGEMENT

The authors would like to express appreciation to financial supports from Project funded by Qingdao Postdoctoral Researchers Applied Research Foundation (2016119), Project funded by China Postdoctoral Science Foundation (2016M602164).

REFERENCES

[1] SV Deshpande.Innovation in robotic surgery: the Indian scenario. Journal of Minimal Access Surgery, 2015, 11(1):106-110.

[2] FPugin, P Bucher and P Morel. History of robotic surgery: From AESOP and ZEUS to Da Vinci. Journal of Visceral Surgery, 2011, 148(5):e3-e8.

[3] Jie Chen and Henry Y K Lau. Transferring autonomous reaching and targeting behaviors for cable-driven robots in minimally invasive surgery.2016 IEEE International Workshop on Advanced Robotics and its Social Impacts (ARSO): IEEE, 2016:79-84.

[4] Miyamoto S, SugiuraM, WatanabeS, etal.Development of minimally invasive surgery systems. Hitachi Review, 2003, 52(4):189-195.

[5] SimaanN, Taylor R H, Flint P.A Dexterous System for Laryngeal Surgery. Proceedings of the 2004 IEEE International Conference on Robotics & Automation. New Orieans, USA, 2004:351-357.

[6] Simaan N, Bajo A, Reiter A, et al. Lessons learned using the insertable robotic effector platform (IREP) for single port access surgery. J Robot Surg, 2013, 7(3):235-240.

[7] Niu G, Pan B, Zhang F, et al. Dimensional synthesis and concept design of a novel minimally invasive surgical robot. Robotica, 2018, 36(5):1-23.

[8] Yan Z, Du Z, Zhang F, et al. Preoperative optimization of the surgical robot considering internal diversity of workspace. ARCHIVE Proceedings of the Institution of Mechanical Engineers Part C Journal of Mechanical Engineering Science 1989-1996 (vols 203-210), 2017, 232(6):095440621769901.

[9] Dehghani M, Moghadam M M, Torabi P. Analysis, optimization and prototyping of a parallel RCM mechanism of a surgical robot for craniotomy surgery. Industrial Robot, 2017, 45(2).

[10] Zhang F, Yan Z, Du Z. Preoperative planning for the multi-arm surgical robot using PSO-GP-based performance optimization.IEEE International Conference on Robotics and Automation. IEEE, 2017.

[11] Leroy N, Kokosy A M, Perruquetti W. Dynamic modeling of a parallel robot. Application to a surgical simulator.IEEE International Conference on Robotics and Automation, 2003. Proceedings. ICRA. IEEE, 2003:4330-4335 vol.3.

[12] Yang J, Yu L, Zhang N, et al. Dynamic modeling and analysis of laparoscope arm for Minimally Invasive Surgical Robot.IEEE International Conference on Mechatronics and Automation. IEEE, 2017:541-546.

[13] Pisla D, Gherman B G, Suciu M, et al. On the Dynamics of a 5 DOF Parallel Hybrid Robot Used in Minimally Invasive Surgery. 2010, 5:691-699.

[14] Gherman B, Pisla D, Vaida C, et al. Development of inverse dynamic model for a surgical hybrid parallel robot with equivalent lumped masses. Robotics & Computer Integrated Manufacturing, 2012, 28(3):402-415.

[15] Chen X, Liang X, Deng Y, et al. Rigid Dynamic Model and Analysis of 5-DOF Parallel Mechanism. International Journal of Advanced Robotic Systems, 2015, 12(7):1.

[16] Yang J, Yu L, Wang L, et al. Dynamic modeling and analysis of the instrument arm based on the physical properties of soft tissues. ARCHIVE Proceedings of the Institution of Mechanical Engineers Part C Journal of Mechanical Engineering Science 1989-1996 (vols 203-210), 2017:095440621771566.

[17] Liu S, Farah E. Multibody Dynamics Modeling and Simulating Using Maple and Maplesim. International Journal of Control & Automation, 2017, 10(5):83-92.

[18] Xu Y, Liu R. Dynamic modeling of constrained planar multibody systems: A case of lower limbs rehabilitative robot. Journal of Mechanical Science & Technology, 2018, 32(7):3389-3394.

[19] Li X, Sun H X, Liao L J, et al. Modeling and Simulation Research of Kane Dynamics Method for the 5-DOF Modular Industrial Robot. International Conference on Information System and Artificial Intelligence. IEEE, 2017:124-128.

[20] Hussain Z, Azlan N Z. KANE's method for dynamic modeling. IEEE International Conference on Automatic Control and Intelligent Systems. IEEE, 2017:174-179.

[21] Jinno M. Proof of concept for a wrist mechanism for articulated forceps for use in robot-assisted laparoscopic surgery. Robomech Journal, 2018, 5(1):5.

[22] Romano A, D'Amore D, Esposito G, et al. Characteristics and Outcomes of Laparoscopic Surgery in patients with large hiatal hernia. A single Center study. International Journal of Surgery Case Reports, 2018.

[23] Jeong S Y, Jin W L, Choi S H, et al. Single-incision laparoscopic cholecystectomy using instrumental alignment in robotic single-site cholecystectomy. Annals of Surgical Treatment & Research, 2018, 94.

[24] Zhang Y, Gandhi M, Birchall C, et al. Single-incision laparoscopic abdominal cerclage placement: a retrospective study of single-port and robotic single-port versus multiport laparoscopy. International Journal of Gynaecology & Obstetrics the Official Organ of the International Federation of Gynaecology & Obstetrics, 2018.

[25] Zimmerman A M, Roye D G, Charpentier K P. A comparison of outcomes between open, laparoscopic and robotic pancreaticoduodenectomy. Hpb the Official Journal of the International Hepato Pancreato Biliary Association, 2018, 20(4):364.

[26] Zihni A, Gerull W D, Cavallo J A, et al. Comparison of precision and speed in laparoscopic and robot-assisted surgical task performance. Journal of Surgical Research, 2018, 223:29.

[27] Tang D., Yin L., Ullah I. Product Design as Integration of Axiomatic Design and Design Structure Matrix. In: Matrix-based Product Design and Change Management. Springer, Singapore, 2018.

[28] Sun J D, Cao G Z, Li W B, et al. Analytical inverse kinematic solution using the D-H method for a 6-DOF robot. International Conference on Ubiquitous Robots & Ambient Intelligence, 2017.

[29] Cui Zuo, Jiang Hongzhou. Design and Implementation of Thunniform Robotic Fish with Variable Body Stiffness. International Journal of Robotics & Automation, 2017, 32(2): 109-116.

[30] Liu Y, Li B, Xu P, et al. Stiffness Modeling and Optimization Analysis of a Novel 6-DOF Collaborative Parallel Manipulator. Intelligent Robotics and Applications. Springer International Publishing, 2014.